



# Characterization and Iron Removal Enhancement of El-Zaafarana White Sand

Amr F. M. Ibrahim<sup>1</sup> · Ahmed A. S. Seifelnassr<sup>1</sup> · Ahmed Al-Abady<sup>1</sup> · Montaser S. El-Salmawy<sup>1</sup> · Abdeaziem M. Abdelaal<sup>1</sup>

Received: 16 June 2022 / Accepted: 3 August 2022 / Published online: 30 August 2022  
© The Author(s) 2022

## Abstract

Iron is a key detrimental impurity in silica sands that determines their contribution to high-technology industries. Herein, a simple ecologically sound approach is investigated for iron removal from a silica sand sample obtained from the El-Zaafarana area-Egypt. The sample was subjected to a detailed microscopic mineralogical study supported by XRD and XRF characterization. The sample was beneficiated using distilled water attrition scrubbing and screening over a 25  $\mu\text{m}$  sieve followed by leaching using a mixture of equal amounts of phosphoric and oxalic acids. Leaching experiments were designed and analyzed using the Box-Behnken design (BBD) methodology. A model was developed and evaluated using the analysis of variance technique to map the relationship between the residual iron oxide in the produced concentrate and selected variables such as leaching temperature, oxalic acid, and phosphoric acid concentrations. XRD and mineralogical analysis reveal that quartz is the most dominant constituent of the studied sand and other minerals such as kaolinite, iron oxide, rutile, and zircon exist in trace amounts. The head sample shows a silica and iron oxide content of 95.69% and 2379 ppm, respectively. Attrition and separation over a 25  $\mu\text{m}$  sieve increase the silica content to 97.05% and decreases the residual iron oxide to 455 ppm. The final product after leaching under optimized conditions shows 99.82% silica and 55 ppm iron oxide.

**Keywords** El-Zaafarana white sand—Egypt · Phosphoric acid · Oxalic acid leaching · Iron removal · Box-Behnken design

## 1 Introduction

The last decade has witnessed exceptional demand for high-purity quartz ( $\text{SiO}_2$ ) as an essential material for many high-tech applications such as semiconductor chips and circuits; optical fibers; solar panels; and aerospace and advanced ceramic materials [1, 2]. The term high purity quartz refers to quartz with less than 50-ppm associated impurities [1], while silica sands represent a weathered derivative of quartz, mainly composed of quartz grains and other impurities. Very high-purity quartz is mined from a few localities in the world, and thus with the expected growth in demand, efficient eco-friendly beneficiation techniques to remove silica sand impurities are of significant consideration.

The majority of silica sand upgrading studies have focused on iron removal to prevent the undesired color and property changes in the final quartz products [3]. Accordingly, different physical, chemical, physico-chemical, and biological beneficiation methods have been investigated [3, 4]. Combinations of these methods are sometimes utilized to improve the quality of sand samples [5]. Chemical leaching was reported by different research groups to induce higher iron removal efficiency when the iron is non-liberated and embedded inside or attached to the surface of sand grains [6]. Various organic [7, 8] and mineral [9–11] acids have been investigated for iron removal from silica sands. Among organic acids, oxalic acid is found to be the most promising because of its complexation and reduction ability [12–15]. Also, phosphoric acid surpasses hydrochloric, sulfuric, nitric, and oxalic acids in leaching iron under the same conditions [16, 17]. Moreover, mixing organic and mineral acids was reported as an effective approach to improve iron removal efficiency and reduce the high cost as well as the environmental concerns of mineral acids [16, 18]. Ultrasound was also introduced as a powerful tool that

✉ Amr F. M. Ibrahim  
Amr.Ibrahim@suezuni.edu.eg

<sup>1</sup> Mining Engineering Department, Faculty of Petroleum and Mining Engineering, Suez University, Suez 43512, Egypt

could assist mineral/organic acid leaching studies [18, 19]. Although the leaching time may become shorter, the leaching process becomes more complicated and difficult to scale up for industrial purposes. Also, it was reported that the leaching temperature and acid concentration parameters were more effective than the leaching time and ultrasound power parameters in iron removal from quartz [18].

Herein, we investigated the effect of using a mixture of phosphoric and oxalic acids on the iron removal efficiency for a white sand sample obtained from El-Zaafarana area—Egypt. Experiments were designed and analyzed using Box-Behnken design (BBD) methodology, and the effect of the leaching parameters such as the leaching temperature; oxalic acid and phosphoric acid concentrations were investigated. El-Zaafarana area, sometimes called Wadi El-Dakhl is one of the most important and strategic white sand localities in the northern part of the Eastern Desert of Egypt, with about 10-million-ton silica sand reserves [20]. Based on the best of our knowledge, only one beneficiation study was found on the beneficiation of silica sand from El-Zaafarana area using oxalic acid leaching, and the sample was essentially a very high-grade one ( $\text{SiO}_2$ : 99.441%) [21]. Enhancing the technical qualification of the Egyptian white sand will support the production for internal or external markets and disclose their potential industrial applications.

Moreover, acid mixtures of oxalic acid with sulfuric acid [22, 23] and hydrochloric acid [18] have been tested before. However, to date, little information is available in the literature on the application of a mixture of phosphoric and oxalic acids to remove iron impurities from silica sand. This gap will be fulfilled only with further studies. The phosphoric/oxalic mixture is expected to be effective and eco-friendly based on the results of previous studies with them as individual acids [13, 16, 17]. Unlike previous studies [18], each acid concentration is considered a variable to disclose the synergistic effect of oxalic and phosphoric acids. The objective of this study is to provide an in-depth characterization of El-Zaafarana silica sand and develop a better understanding of the effectiveness of phosphoric/oxalic acid mixture for iron removal from silica sand in terms of leaching parameters.

## 2 Material and Methods

### 2.1 Materials

The silica sand samples used in this work were obtained from El-Zaafarana area, Wadi-El-Dakhl, Eastern Desert, Egypt. The area covers about 2880 km<sup>2</sup> between latitudes 28° 30' and 28° 55' N and longitudes from 32° 20' to 32° 50' E. The area contains a reserve of about 10 M tons of loose or friable materials without rock cover [20]. The white sand at Wadi El-Dakhl belongs to Malha Formation

(Early Cretaceous age), about 100 m thick composed mainly of pure white sands in horizontal beds mutual with some intercalation of kaolinite and sandstones [24]. The obtained samples were mixed and homogenized to prepare a representative sample for mineralogical, chemical, and beneficiation work. Oxalic acid ( $\text{C}_2\text{H}_2\text{O}_4 \cdot 2\text{H}_2\text{O}$ , > 99%, from Alpha Chemika, CAS# 6153–56-6) and phosphoric acid ( $\text{H}_3\text{PO}_4$ , 85% from Alpha Chemika, CAS# 7664–38-2) were used for leaching experiments diluted with distilled water.

### 2.2 Characterization

The size distribution of the bulk sample and the attrition product were determined by mechanical sieving. The as-received sample was dry-sieved, while the attrition product was wet-sieved using Fritsch shaker, according to the German standards as described in earlier publications [25, 26]. The sand fractions were dried at 105 °C for 24 h and then weighted. Leica MZ6, stereo-microscope (Leica-Germany) equipped with Leica Application Suite EZ software was used to study the minerals composing the as-received sand sample. Thin section images for the as-received sample were taken using Olympus System Microscope Model BX41. The X-ray diffraction (XRD) patterns for the as-received and –25- $\mu\text{m}$  attrition samples were collected using a PANalytical X'Pert PRO X-ray diffractometer operated at 40 kV and 30 mA with  $2\theta$  ranging from 5 to 50 using Cu K $\alpha$  radiation. The chemical analyses for the as-received and treated silica sand samples were obtained using a Rigaku supermini 200 X-ray fluorescence spectrometer.

### 2.3 Attrition and Leaching Experiments

The as-received silica sand was subjected to attrition scrubbing experiments. Attrition was conducted to remove clay minerals and dust covering silica grains which could increase reagent consumption. Attrition experiments were carried out in a 2-L glass beaker where a 250-g sand sample was added to 1000 mL distilled water (20% solids). The pulp was stirred for 30 min using an overhead mechanical stirrer with a plastic impeller adjusted at 3000 rpm. The whole pulp was then wet sieved over a 25  $\mu\text{m}$  sieve to exclude clay minerals and fine-grain impurities. The collected sand particles (+ 25  $\mu\text{m}$ ) were washed repeatedly with distilled water and dried at 105 °C for 24 h. The (– 25- $\mu\text{m}$ ) fraction was left for 1 day so that the solids settle down, and most of the water can be removed by decantation. The (– 25  $\mu\text{m}$ ) solids are then collected by filtration and then dried at 105 °C for 24 h. The separated fractions were characterized using XRD and XRF.

Leaching experiments were conducted in 250-ml-conical glass flasks using an agitating laboratory incubator. The incubator is heated until it reaches a preset temperature (35, 55 or 75 °C). About 10 g washed and dried (+ 25 μm) silica sample and a mixture of oxalic and phosphoric acids with different concentrations and equal volumes (25 mL each) were mixed in the glass flasks. The flasks were then tightly sealed and fixed in their holders inside the incubator. The leaching process is then conducted for 2 h at 400 rpm. After the experiment, the sand particles from each run were collected by filtration, washed each with 250 mL distilled water, and finally dried at 105 °C for 24 h before being sent for analysis. The iron oxide removal efficiency was calculated for the sand product after the leaching process using Eq. (1).

$$Fe_2O_3 \text{ removal efficiency (\%)} = \left[ 1 - \frac{\text{Residual iron oxide percentage after leaching}}{\text{Iron oxide percentage in attrition product}} \right] \times 100 \tag{1}$$

### 2.4 Box-Behnken Design Methodology

Leaching experiments were designed using the Box-Behnken Design method, a commonly preferred design of Response Surface Methodology that is frequently used in silica leaching studies [17, 18]. Three key independent variables including temperature (35–75 °C), concentrations of oxalic acid (0.02–0.2 M), and phosphoric acid (0.02–0.2 M) were chosen for investigation at three different levels determined based on literature and preliminary experiments. The agitation speed is taken as the maximum on the incubator, 400 rpm, while the time, 2 h, is considered good enough for the completion of the leaching process based on preliminary experiments. The iron oxide content of the concentrate was considered the response factor. The data obtained for the iron oxide content, were fitted to a second-order polynomial model, (see Eq. (2)) [18, 27]:

$$Response = \epsilon_0 + \sum_{i=1}^3 \epsilon_i X_i + \sum_{i=1}^3 \epsilon_{ii} X_i^2 + \sum_{i=1}^2 \sum_{j=i+1}^3 \epsilon_{ij} X_i X_j \tag{2}$$

where  $\epsilon_0$ ,  $\epsilon_i$ ,  $\epsilon_{ii}$ , and  $\epsilon_{ij}$  are for the intercept, linear, square, and interaction regression coefficients respectively.  $X_i$  and  $X_j$  are the independent variables ( $i \neq j$ ). Subsequent regression analysis using analysis of variance, ANOVA, and generation of response surface plots were done using Expert Design V. 13.0.5.0 statistical software to assess the statistical significance of the model relating the selected leaching variables to the measured response. Finally, the resulting correlation was introduced into an optimization software (LINGO V.14) to identify the optimal values for the

variables that minimize the residual iron oxide content of the leaching product [28]. The results are finally compared with the optimum conditions for the tested variables.

## 3 Results

### 3.1 El-Zaafarana Sand and Attrition Product Characteristics

The XRD patterns of El-Zaafarana bulk sand sample and the (– 25-μm) washed sample are given in Fig. 1. The as-received sample only shows diffraction peaks only from quartz [21], while extra peaks appear when the sample is washed and screened over the 25 μm sieve. This indicates

that the sand sample is composed mainly of quartz and minor quantities of kaolinite, calcite, and probably other very low proportion of other minerals that could not be detected by XRD. This comes with a great match with the XRD results reported earlier for El- Zaafarana sand [29].

The mineralogical study gave more details about the type of minor impurities associated with the sand grains. Optical microscope images for the as-received sand sample are given in Fig. 2(A–C). The sample consists essentially of quartz associated with minor amounts of feldspars and rare amounts of rutile, zircon, heavy silicates, mica, iron oxides, and opaque minerals. Quartz grains are very fine to fine-grain, well-sorted, and rounded to subangular in shape. The grains are transparent, colorless to pale pink. The surface textures

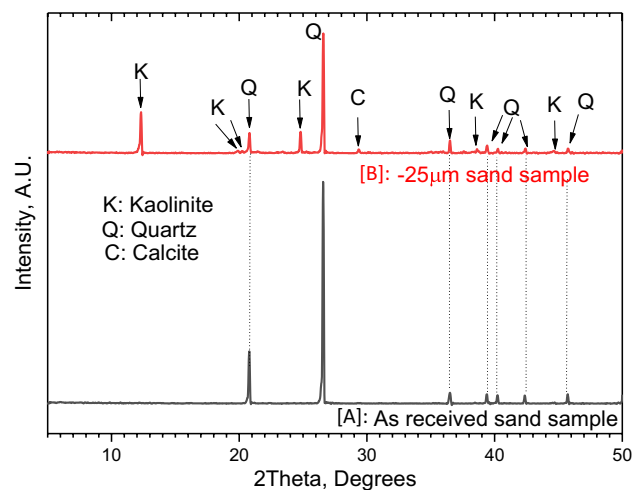
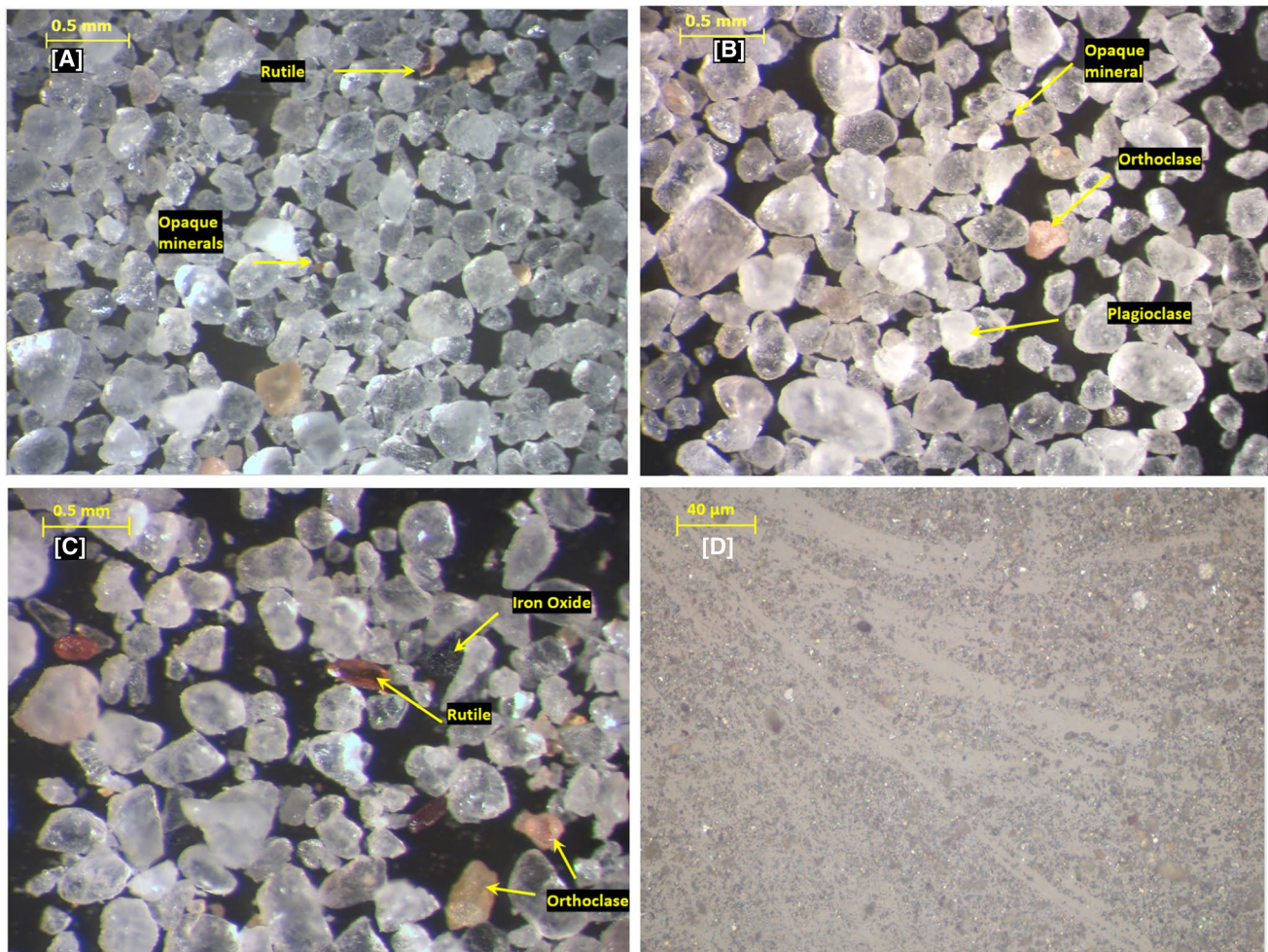


Fig. 1 XRD patterns of El-Zaafarana sand: [A] As-received and [B] (– 25 μm) washed sample



**Fig. 2** Optical microscope images of El-Zaafarana as-received silica sand sample [A–C] and (–25µm) rejected fraction [D]

of the quartz grains suggest that they are the product of mechanical weathering [30]. The opaque fine to very fine brown grains could be attributed mainly to iron oxides [31]. Feldspars (plagioclase and potash feldspar) are very fine to fine-grained, subrounded to subangular in shape, and translucent white to orange in color. Some heavy minerals could also be found such as rutile and zircon. Rutile is very fine-grained, elongated, rounded, and has a characteristic red color. Zircon is found as colorless, very fine-grained prismatic crystals.

El-Zaafarana as-received sample was also imaged as a thin section and the obtained images are given in Fig. 3(A–D). A dominance of quartz grains with a shape varying from angular to well-rounded grains was observed. Iron oxide and kaolinite were found as discrete particles and as stains on the surface of some of the transparent quartz grains. Also, composite quartz grains are found cemented with an opaque material that could be kaolinite and/or iron oxides [21] such as those noticed in Fig. 3C. Other quartz

grains are found with cracks filled with the cementing materials, as shown in Fig. 3D.

The composition of El-Zaafarana sand sample was further determined by XRF analysis. Silica and other minor phases are expressed as oxides in Table 1. Silica was the dominant component approaching 95.69%, and other oxides such as alumina and calcium oxide come next confirming the existence of kaolinite and calcite as detected by XRD. Aluminum, sodium, potassium, and calcium may also result from orthoclase and plagioclases feldspars. The presence of iron, magnesium, titanium, and zirconium confirms the existence of minerals such as hematite, dolomite, rutile, and zircon. Other very rare phases such as yttrium oxide and hafnium dioxide were also detected.

Attrition scrubbing tests were carried out to detach clay and other impurities coating the silica grains. The attrition product is further screened on a 25 µm sieve to reject most of the fine particles and clays. The dry mechanical sieving of the as-received sample and the

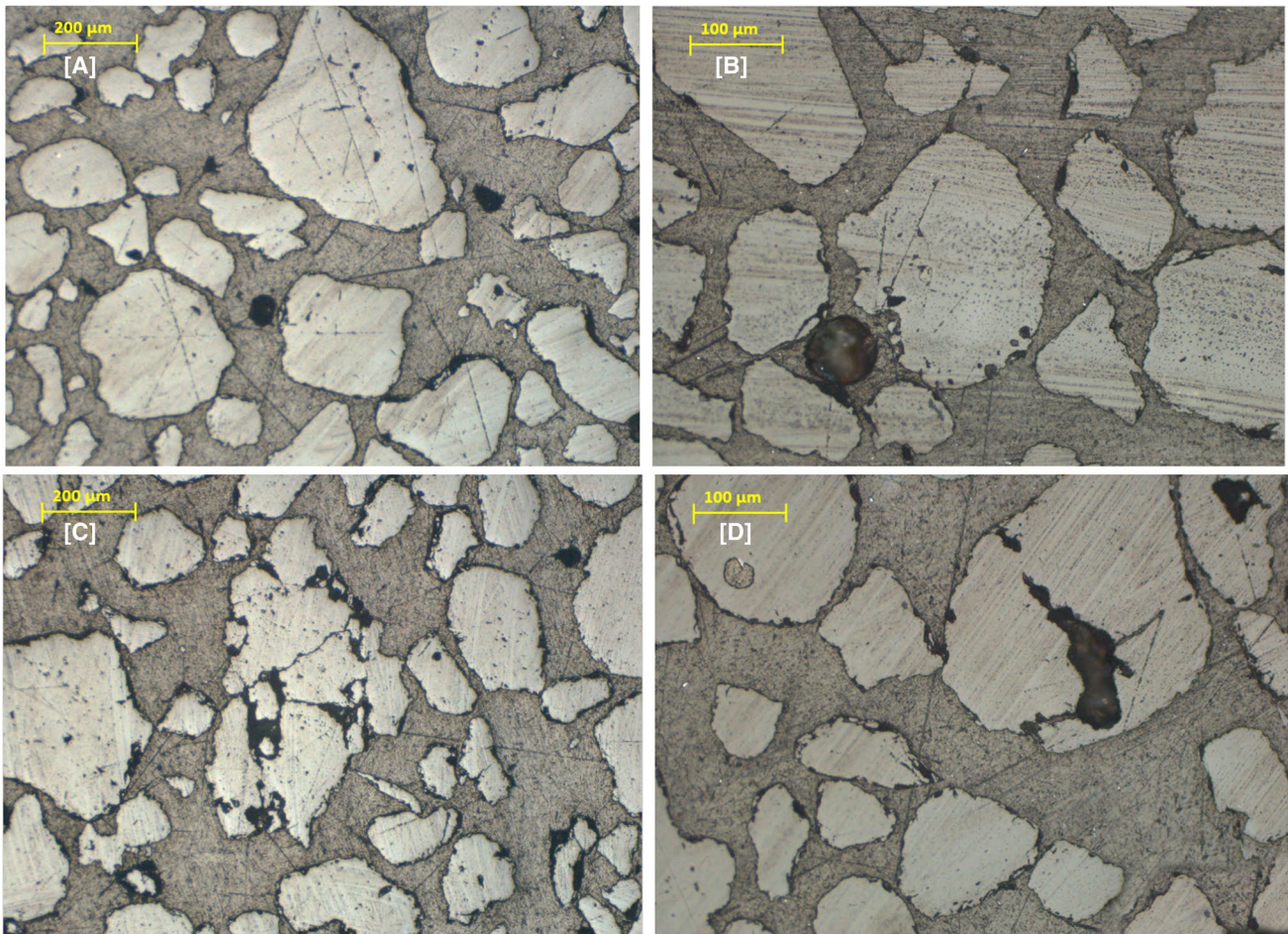


**Fig. 3** Thin section images of El-Zaafarana as-received silica sand sample

attrition product are compared in Table 2. The size fraction ( $-300 + 180$ )  $\mu\text{m}$  represents the mode size of the sample. The mean particle size,  $D_{50}$  is about 270  $\mu\text{m}$  and about 95% of the grains lie in the range between 630 and 90  $\mu\text{m}$ . The water washing of the attrition product facilitates the collection of fine-sized particles and detachable mineral coatings from the surfaces of the silica grains. Some composite silica particles may also break into smaller particles during the particle collision in the attrition process. This explains the reduction of the retained weight in all size fractions and their accumulation in the finest sized fractions ( $-90 + 25$ ) and  $-25 \mu\text{m}$  as given in Table 2.

The XRD patterns in Fig. 1 for the ( $-25\text{-}\mu\text{m}$ ) sample show enrichment of the rejected fraction in kaolinite and calcite. Also, the majority of the fine-grained colored and opaque minerals are collected in the ( $-25\text{-}\mu\text{m}$ ) fraction, as imaged in Fig. 2D. The chemical analysis of the washed fraction after attrition and separation over  $+25 \mu\text{m}$  is given in Table 1. The data show an upgrade in the sand quality of the ( $+25\text{-}\mu\text{m}$ ) sample compared to the as-received head

sample. The silica content has increased from 95.69% in the as-received sample to 97.05% in the attrition product. Iron oxide and alumina show a significant reduction after attrition  $\sim 70\text{--}80\%$ . The rejection of kaolinite and fine-grained iron oxide particles to the ( $-25 \mu\text{m}$ ) fractions explains the increase in alumina in the reject. Attrition also leads to a considerable decrease in the content of the other phases of impurities in the silica sample.

### 3.2 BBD Design and Leaching Results

The experimental BBD design variables and response for the residual iron oxide in the leaching product are given in Table 3. Each row in Table 3 represents a leaching experiment at conditions with a level of the chosen factors, and the corresponding response was also reported. A second-order quadratic polynomial model was selected to express the correlation between the chosen independent variables and the measured response. The model after eliminating the statistically insignificant terms is represented in uncoded and coded units by Eqs. (3) and (4). The symbols *A*, *B*, and *C* refer to

**Table 1** The complete chemical analysis of the as-received and (+25 µm) attrited silica samples as well as the leaching concentrate at the enhanced leaching conditions

Component	As-received sample	Attrited (+25-µm) sample	Concentrate at best leaching conditions
SiO <sub>2</sub>	95.6962	97.0481	99.8221
Fe <sub>2</sub> O <sub>3</sub>	0.2379	0.0455	0.0055
Al <sub>2</sub> O <sub>3</sub>	0.6619	0.1921	0.0221
CaO	1.2692	0.8830	0.0134
MgO	0.7958	0.6995	0.0314
Na <sub>2</sub> O	0.2986	0.2650	0.0075
K <sub>2</sub> O	0.1942	0.1521	0.0082
Cr <sub>2</sub> O <sub>3</sub>	0.0968	0.0827	0.0208
TiO <sub>2</sub>	0.3954	0.3853	0.0186
MnO	0.0375	0.0214	0.0137
SO <sub>3</sub>	0.0568	0.0491	0.0033
Cl	0.0549	0.0437	0.0039
ZrO <sub>2</sub>	0.0726	0.0345	0.0087
Y <sub>2</sub> O <sub>3</sub>	0.0375	0.0264	0.0011
NiO	0.0139	0.0102	0.0041
ZnO	0.0594	0.0426	0.0089
HfO <sub>2</sub>	0.0214	0.0189	0.0066

**Table 2** Size distribution of El-Zaafarana as-received sample and attrition product

Size fraction µm	Dry as-received sample		Attrition product	
	Wt. %	Cumulative wt. % passing	Wt. %	Cumulative wt. % passing
+ 710	1.04	98.96	1.02	98.98
– 710+630	1.66	97.30	1.63	97.35
– 630+425	21.81	75.49	19.88	77.47
– 425+300	12.19	63.30	11.78	65.69
– 300+180	49.73	13.57	49.59	16.10
– 180+90	10.95	2.63	12.01	4.09
– 90+25	1.35	1.28	1.46	2.63
– 25	1.28	0.00	2.63	0.00
Total	100.00		100.00	

the concentration of phosphoric acid, the concentration of oxalic acid, and the leaching temperature, respectively.

$$Fe_2O_3(ppm) = 415.65 - 450.00 A + 820.63 B - 0.76 C - 14.17 BC - 4146.83 B^2 \quad (3)$$

$$Fe_2O_3(ppm) = 278.71 - 40.50 A - 78.38 B - 46.38 C - 25.50 BC - 33.59 B^2 \quad (4)$$

Analysis of variance was performed to assess the suitability of the developed model and the effect of the studied

**Table 3** Box-Behnken design variables and measured response in this study

Run	Independent uncoded factors			Response
	A	B	C	
	Phosphoric acid concentration	Oxalic acid concentration	Leaching temperature	Leaching product iron oxide content
	M	M	°C	ppm
1	0.11	0.20	35	185
2	0.11	0.11	55	299
3	0.20	0.11	75	95
4	0.02	0.02	55	289
5	0.20	0.02	55	132
6	0.02	0.11	35	360
7	0.02	0.20	55	296
8	0.11	0.11	55	295
9	0.11	0.11	55	340
10	0.02	0.11	75	300
11	0.11	0.02	35	170
12	0.20	0.20	55	280
13	0.11	0.20	75	258
14	0.20	0.11	35	255
15	0.11	0.02	75	358

variables. The high value for the *F*-value and the very low *p*-value ( $<<0.05$ ) for the model indicates that the model and model terms are significant [18, 27, 32]. A good model fit would yield a coefficient of determination ( $R^2$ ) value of at least 0.8 [18]. As presented in Table 4, the model shows  $R^2$  close to 1 (0.9561), indicating that only less than 0.0439 of the total variations were not explained by the model and suggesting a pretty good correlation between the measured response and the independent variables [18, 27]. The adj- $R^2$  and pred- $R^2$  values are 0.9318 and 0.8685, respectively. The difference between these two values is less than 0.2, this indicates that the model has good predictability [18, 32].

A lack of fit *p*-value ( $>0.05$ ) is an indication that the lack of fit of the developed model is insignificant relative to the pure error, and this further supported the acceptability of the model [18, 32]. “Adequate precision” measures the signal-to-noise ratio. A ratio greater than 4 is desirable [18, 32]. The relationship between the actual experimental results and the predicted values for the iron oxide of the leaching product are presented in Fig. 4A. The fact that the predicted points fall very close to the 45° line justifies that the developed model fits very well with the experimental data. The plot of the predicted values vs. residuals in Fig. 4A shows that the data are distributed throughout the plot without exceeding the lower and upper limit values. A good agreement

**Table 4** Analysis of variance of the reduced quadratic model developed in this work for the residual iron oxide in the leaching product

Source	Degree of freedom	Sum of squares	Mean square	F-value	p-value
Model	5	86,281.35	17,256.27	39.23	< 0.0001
A—phosphoric acid	1	13,122.00	13,122.00	29.83	0.0004
B—oxalic acid	1	49,141.13	49,141.13	111.71	< 0.0001
C—temperature	1	17,205.13	17,205.13	39.11	0.0001
B × C	1	2601.00	2601.00	5.91	0.0379
B <sup>2</sup>	1	4212.10	4212.10	9.58	0.0128
Residual error	9	3959.05	439.89		
Lack-of-fit	7	3778.39	539.77	5.98	0.1508
Pure error	2	180.67	90.33		
Correction total	14	90240.40			
Fit statistics			R <sup>2</sup>		0.9561
			Adjusted R <sup>2</sup>		0.9318
Adequate precision	20.4083		Predicted R <sup>2</sup>		0.8685

between actual and predicted data occurs when the residual errors are less than 2% [18, 32].

Surface and contour response plots for the model devolved in this work for the iron oxide in the leaching product are drawn to better visualize the effects of independent parameters and their interactions. Each figure is drawn while maintaining one parameter constant at an intermediate value of the test range, and the effects of the other two variables were addressed. The effect of phosphoric and oxalic acids on the residual iron oxide of El-Zaafarana sand is given in Fig. 5A in the form of surface and contour plots. Those plots are drawn while keeping the temperature constant at 55 °C. It

is obvious from the figure that increasing the concentration of any of the acids will result in a reduction of the residual iron oxide. From the slope and the value of the coefficients of both acids in Eq. (4), oxalic acid seems more effective in removing iron oxide from the studied silica samples. The residual iron oxide is not significantly affected by the mutual interactions of both acids. For example, if we consider a mid-point at the surface of Fig. 5A, [0.11 M phosphoric acid, 0.11 M oxalic acid, and 55 °C], the residual iron oxide in the concentrate is 278 ppm, i.e., representing 38.7% iron removal efficiency. By increasing phosphoric acid concentration to 0.2 M at 0.11 M oxalic acid, the iron removal efficiency

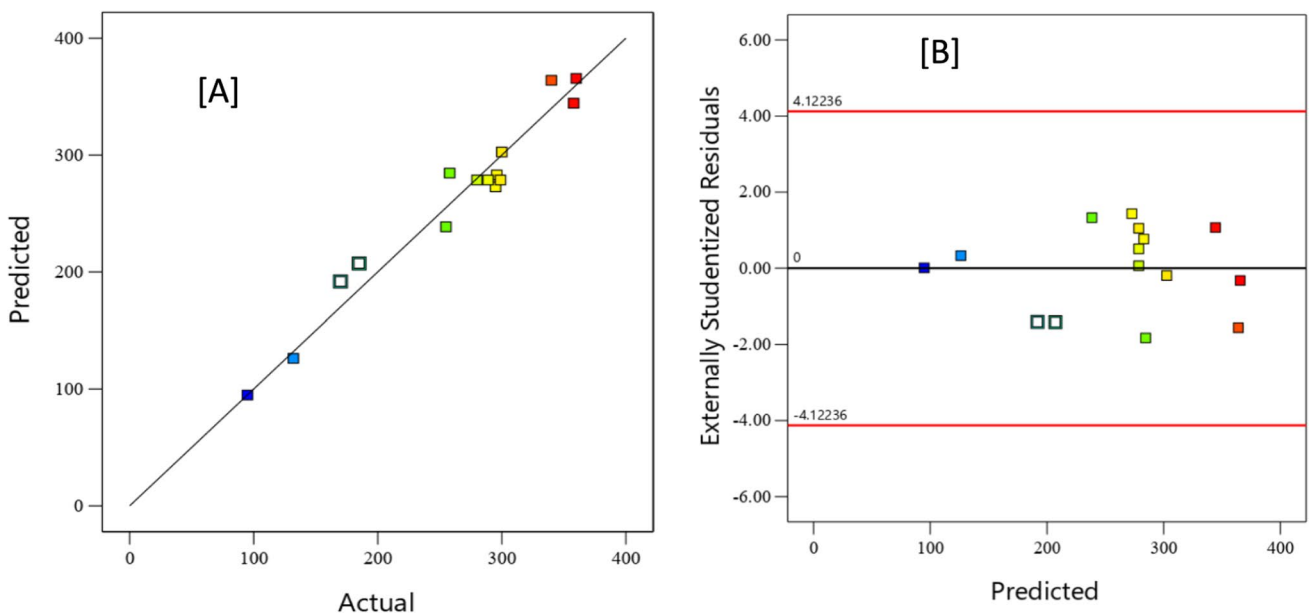


**Fig. 4** Residual plots for the predicted iron oxide content of the leaching product: (A) predicted vs actual values and (B) residuals vs predicted values

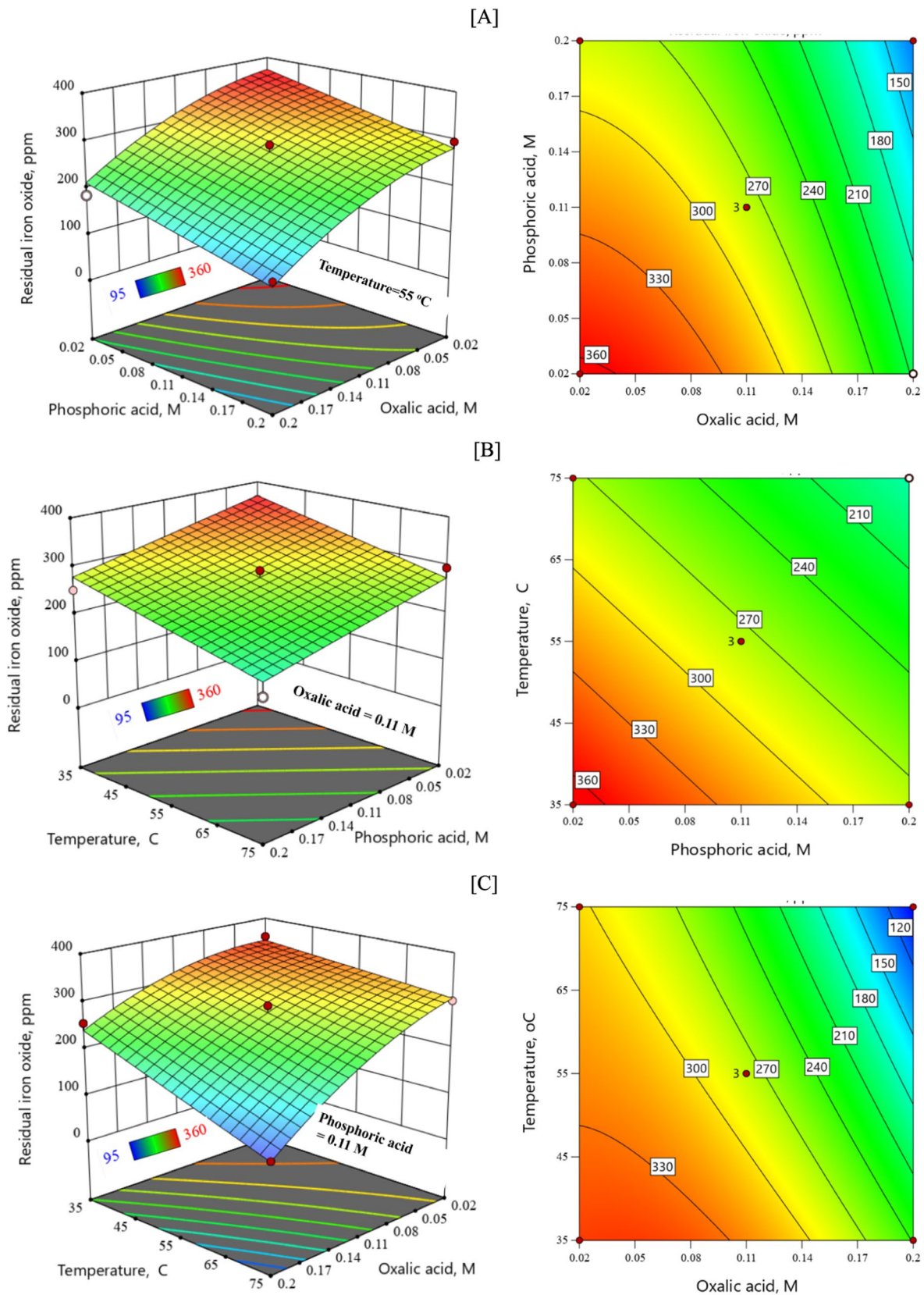


**Fig. 5** Typical surface and contour plots for the effect of independent variables on the iron oxide in the leaching product. (A) phosphoric acid concentration vs. oxalic acid concentration at 55 °C. (B) phos-

phoric acid concentration vs. leaching temperature at an oxalic acid concentration of 0.11 M. (C) oxalic acid concentration vs. leaching temperature at a phosphoric acid concentration of 0.11 M

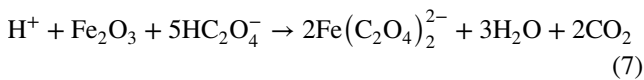
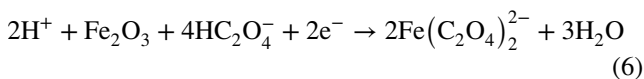
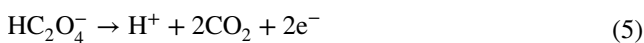


increases to 47.6% (8.9% enhancement in iron removal efficiency). Increasing oxalic acid concentration to 0.2 M at 0.11 M phosphoric acid increases the iron removal efficiency to 63.4 (24.6% enhancement in iron removal efficiency). Increasing both acid concentrations to 0.2 M, increases the iron removal efficiency to 72.3%. The enhancement in the iron removal efficiency, in this case, is 35.5%~the sum of individual effects of the acids.

The effect of temperature on the reactivity of each acid, while maintaining the other at a mid-way concentration of 0.11 M is given in Fig. 5B and C. As illustrated in both figures, increasing temperature causes an increase in the leaching rate and enhances the iron removal efficiency. Again, the mutual interactions of temperature and phosphoric acid are negligible, and the iron oxide content is affected mainly by the variables themselves. On the other hand, the interactions between temperature and oxalic acid are quite significant. From the slope of the surface and coefficients of the model equation in coded form, oxalic acid shows the major effect among the studied variables. Temperature shows a slightly higher effect on the iron removal efficiency compared to phosphoric acid.

EL Sayed et al. [23] also reported insignificant mutual interactions between sulfuric acid and oxalic acid in their leaching experiments of Wadi Qena kaolinitic sand. Also, the sulfuric acid effect on iron removal was insignificant in leaching experiments of quartz using a mixture of sulfuric acid and oxalic acid [22]. More interestingly, the interaction effect of H<sub>2</sub>SO<sub>4</sub> concentration with oxalic acid was found to be negative, and the most valuable interaction effect on iron oxide removal was observed between oxalic acid and temperature [22].

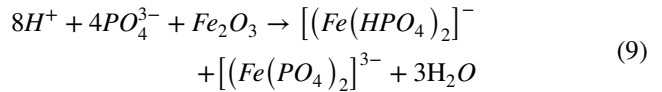
The removal of iron from silica sand with oxalic acid has been studied by several authors [22, 33, 34]. Iron removal takes place in a reducing mechanism with oxalate being oxidized to form carbonic acid or carbon dioxide and iron oxide is reduced to form Fe(II)-oxalate (Eqs. (5–7)).



This redox reaction suggests that hydrogen ions, oxalate, and iron oxide participate in the leaching process. At a given iron oxide mineralogy and its particle size, the dissolution kinetics is influenced by oxalate concentration [22, 33, 34].

On the other hand, the phosphoric acid in water provides H<sup>+</sup> ions that are adsorbed on the surface of iron oxides creating surface-active centers on which the main reaction for dissolution takes place (Eq. (8)) [16, 35, 36]. Increasing hydrogen ion concentration will lead to more hydrogen ion adsorption which

in turn will increase the number of active centers and finally the dissolution rate will increase. H<sub>3</sub>PO<sub>4</sub> ionization provides not only more hydrogen ions but, the phosphate ions also adsorb on activated surfaces and release ferrous and ferric species as Fe-phosphate complexes in ionic form as given in Eq. (9) [16, 35, 36].



The results also show an increase in iron removal as a function of the leaching temperature. This phenomenon is attributed to the fact that temperature increase will lead to an increase in both the reaction rate and diffusion rate of reactants and reaction products [13, 16, 17, 37]. The present results contradict the conclusion Zhang et al. [16] that phosphoric acid is more effective than oxalic acid in the purification of iron impurities from quartz sand. By returning to their work, we found that phosphoric acid was effective compared to oxalic acid only in concentrations ≥ 0.5 M and one data point at ~0.1 M showed that both phosphoric and oxalic acids behave similarly. The reduction of the iron removal efficiency by oxalic acid at higher concentrations is attributed to the formation of more oxalates that form a product layer around the mineral coatings, which decreases the leaching rate [13, 22, 23]. Also, Hernández and coworkers reported that phosphoric acid must be thermally activated above 80 °C, [35] to be effective and the experiments in this work were conducted at a temperature maximum of 75 °C.

### 3.3 Enhancement of the Leaching Process and Potential Industrial Uses

Enhancement of the results aims to determine the experimental conditions at which the leaching product contains the least iron oxide. The best operating conditions determined in this work for the leaching process are 0.2 M oxalic acid, 0.2 M phosphoric acid at 75 °C. Same results were obtained using the Design-Expert software desirability approach and LINGO. The minimum predicted iron content at these conditions is 54 ppm. A control experiment conducted under these conditions showed quite small differences between the measured and predicted iron oxide content in the leaching product, as given in Table 1. These results also confirm the accuracy of the developed model.

The combination of attrition scrubbing and leaching using a mixture of oxalic and phosphoric acids was effective in increasing the quality of El-Zaafarana sand. Based on the data presented in Tables 1 and 2, the yield and recovery after the attrition process are 97.37 and 98.75%. With no loss of silica

sand upon leaching and the dissolution of silica-associated impurities, that exist in minor quantities, the recovery and yield of the whole process are mostly dependent on the attrition process. The final product exhibits a high silica content of 99.82% compared to 95.69% in the as-received sample. The iron content has decreased from 2379 ppm in the bulk sample to 55 ppm for the treated sample. Shaban and AbuKhadr [21] reported that the leaching of a sand sample obtained from El-Zaafarana area using 8 g/ton oxalic acid at 95 °C for 120-min leaching produces a final product of 99.68% SiO<sub>2</sub> and 0.017% iron content. Compared to their results, it appears that conducting the leaching process at a higher temperature is probably a more practical approach to further enhancement of the iron oxide removal efficiency. Increased leaching temperatures will be necessary especially when iron impurity exists in the cracks of the quartz grains [38]. The leaching of El-Zaafarana sand at higher temperatures will be addressed in future studies.

The British Standards (BS 2975) and American Ceramic Society and National Bureau Standard (ACS & NBS) are two well-established standards for the recommended limits for the composition of quartz sand for different glass grades [39]. El-Zaafarana as-received sand sample shows a silica content of 95.69% (i.e., 43,100 ppm impurities). According to the (ACS and NBS), the studied glass sand is not suitable for any of the nine glass categories in the standard because of the relatively high CaO + MgO content (> 0.5%). The as-received sample could be suitable for insulating fibers according to BS 2975 with limitations in grain size requirements (80% of the sand grains should fall between 420 µm and 150 µm). The results obtained in this work showed that attrition scrubbing and leaching of El-Zaafarana sand is required to improve the sand quality to meet the specifications for other categories of silica glass. The final concentrate is suitable for all categories from amber glass to optical glass according to the ACS and NBS. However, according to the BS 2975, the produced concentrate is suitable for insulating fibers, colored container, and flat glass. The high percent of Cr<sub>2</sub>O<sub>3</sub> (0.0208%) suggests that the sand is not suitable for optical, tableware, borosilicate, or colorless glass.

## 4 Conclusions

The mineralogical study and characterization by XRD and XRF of El-Zaafarana white sand sample show that quartz is the most dominant constituent of the sample (95.69%). Other mineral impurities such as kaolinite, calcite, iron oxide, rutile, and zircon exist in trace amounts. Impurities exist as discrete particles, coating or inside silica grain. A substantial upgrade in the chemical properties was realized after attrition scrubbing and separation over the 25 µm sieve due to the rejection of clay and fine-grained crystals. The leaching experiments led to the development of a mathematical model for a satisfactory estimation of residual iron oxide of the leaching concentrate

over a range of selected operating variables, typically the temperature and concentrations of oxalic and phosphoric acid. It was found that oxalic acid and temperature were more effective than phosphoric acid in the enhancement of iron removal efficiency from the silica sand. The best leaching experimental conditions in this work were determined as 0.2 M oxalic acid, 0.2 phosphoric acid, and 75 °C. The final leaching concentrate under these conditions shows a residual iron oxide content of 55 ppm and 99.82% silica which match the requirements of insulating fibers, colored container, and flat glass applications.

**Acknowledgements** The authors would like to thank the Mining Engineering staff members at the Faculty of Petroleum and Mining Engineering for their guidance and valuable comments.

**Author Contribution** Ahmed Al-Abady: conceptualization, performing experiments, and characterization work. Amr Ibrahim: conceptualization, experiment design, formal analysis, data curation, and writing of original draft. Ahmed Seifelnassr, Montaser El-Salmawy, and Abdeaziem Abdelaal: conceptualization, supervision, administration, review, and editing.

**Funding** Open access funding provided by The Science, Technology & Innovation Funding Authority (STDF) in cooperation with The Egyptian Knowledge Bank (EKB).

**Data Availability** The datasets generated during and/or analyzed during the current study are available from the corresponding author on reasonable request.

## Declarations

**Ethics Approval and Consent to Participate** There are no ethical issues associated with this manuscript and all the authors consented to participate.

**Consent for Publication** All the authors consented to the publication of the research article.

**Competing Interests** The authors declare no competing interests.

**Open Access** This article is licensed under a Creative Commons Attribution 4.0 International License, which permits use, sharing, adaptation, distribution and reproduction in any medium or format, as long as you give appropriate credit to the original author(s) and the source, provide a link to the Creative Commons licence, and indicate if changes were made. The images or other third party material in this article are included in the article's Creative Commons licence, unless indicated otherwise in a credit line to the material. If material is not included in the article's Creative Commons licence and your intended use is not permitted by statutory regulation or exceeds the permitted use, you will need to obtain permission directly from the copyright holder. To view a copy of this licence, visit <http://creativecommons.org/licenses/by/4.0/>.

## References

1. Vatalis KI, Charalampides G, Platias S, Benetis NP (2014) Market developments and industrial innovative applications of high purity

- quartz refines. *Procedia Econ Financ* 14:624–633. [https://doi.org/10.1016/S2212-5671\(14\)00751-5](https://doi.org/10.1016/S2212-5671(14)00751-5)
2. Banihashemi F, Ibrahim AFM, Babaluo AA, Lin JYS (2019) Template-free synthesis of highly b-oriented mfi-type zeolite thin films by seeded secondary growth. *Angew Chem Int Ed* 58(8):2519–2523. <https://doi.org/10.1002/anie.201814248>
  3. Haus R, Prinz S, Priess C (2012) Assessment of high purity quartz resources. In: Götze J, Möckel R (eds) *Quartz: deposits, mineralogy and analytics*. Springer Berlin Heidelberg, Berlin, Heidelberg, pp 29–51. [https://doi.org/10.1007/978-3-642-22161-3\\_2](https://doi.org/10.1007/978-3-642-22161-3_2)
  4. Lin M, Liu Z, Wei Y, Liu B, Meng Y, Qiu H, Lei S, Zhang X, Li Y (2020) A critical review on the mineralogy and processing for high-grade quartz. *Min Metall Explor* 37(5):1627–1639. <https://doi.org/10.1007/s42461-020-00247-0>
  5. Santos MFM, Fujiwara E, Schenkel EA, Enzweiler J, Suzuki CK (2015) Processing of quartz lumps rejected by silicon industry to obtain a raw material for silica glass. *Int J Miner Process* 135:65–70. <https://doi.org/10.1016/j.minpro.2015.02.002>
  6. Lin M, Lei S, Pei Z, Liu Y, Xia Z, Xie F (2018) Application of hydrometallurgy techniques in quartz processing and purification: a review. *Metall Res Technol* 115(3):303. <https://doi.org/10.1051/metal/2017105>
  7. Taxiarchou M, Panias D, Douni I, Paspaliaris I, Kontopoulos A (1997) Removal of iron from silica sand by leaching with oxalic acid. *Hydrometallurgy* 46(1):215–227. [https://doi.org/10.1016/S0304-386X\(97\)00015-7](https://doi.org/10.1016/S0304-386X(97)00015-7)
  8. Mohammed M, Güler T, Polat E, Çetin N, Kuşçu Ü (2019) Quartz bleaching by oxalic acid: relationship between rejection rate of impurities and color response. *Türkiye 26 Uluslararası Madencilik Kongresi ve Sergisi*. <http://acikerisim.mu.edu.tr/xmlui/handle/20.500.12809/6339>
  9. Abdelkarim K (2009) Acid leaching technology for obtaining a high-purity of silica for photovoltaic area. *Chem Eng Trans* 17:97–202. <https://doi.org/10.3303/CET0917034>
  10. Kefai A, Sahraoui T, Kheloufi A, Bobociou E (2019) Optimization of quartz sand leaching process using design experiments method (DOE). *Silicon* 11(3):1481–1488. <https://doi.org/10.1007/s12633-018-9966-1>
  11. Mohammed M, Güler T, Polat E (2019) Rejection of iron coloring impurities of quartz ore by sulfuric acid bleaching. Paper presented at the The 26th International Mining Congress and Exhibition of Turkey. <http://acikerisim.mu.edu.tr/xmlui/handle/20.500.12809/6327>
  12. Vegliò F, Passariello B, Abbruzzese C (1999) Iron removal process for high-purity silica sands production by oxalic acid leaching. *Ind Eng Chem Res* 38:4443–4448
  13. Du F, Li J, Li X, Zhang Z (2011) Improvement of iron removal from silica sand using ultrasound-assisted oxalic acid. *Ultrason Sonochem* 18(1):389–393. <https://doi.org/10.1016/j.ultsonch.2010.07.006>
  14. Li J-s, Li X-x, Shen Q, Zhang Z-z, Du F-h (2010) Further purification of industrial quartz by much milder conditions and a harmless method. *Environ Sci Technol* 44(19):7673–7677. <https://doi.org/10.1021/es101104c>
  15. Panias D, Taxiarchou M, Douni I, Paspaliaris I, Kontopoulos A (1996) Thermodynamic analysis of the reactions of iron oxides: dissolution in oxalic acid. *Can Metall Q* 35(4):363–373. <https://doi.org/10.1179/cmqr.1996.35.4.363>
  16. Zhang Z, Li J, Li X, Huang H, Zhou L, Xiong T (2012) High efficiency iron removal from quartz sand using phosphoric acid. *Int J Miner Process* 114–117:30–34. <https://doi.org/10.1016/j.minpro.2012.09.001>
  17. Bas AD (2021) Quartz bleaching by phosphoric acid: an investigation on the relationship between Fe rejection rate and colour response. *Miner Eng* 161:106739. <https://doi.org/10.1016/j.mineng.2020.106739>
  18. Arslan V (2021) The modeling and optimization of iron removal from silica sand under ultrasound-assisted leaching by response surface methodology. *Min Metall Explor* 38(5):2229–2237. <https://doi.org/10.1007/s42461-021-00457-0>
  19. Yang C-Q, Li S-Q (2020) Kinetics of iron removal from quartz under ultrasound-assisted leaching. *High Temp Mater Processes (London)* 39(1):395–404. <https://doi.org/10.1515/htmp-2020-0081>
  20. Ezz-El-Din M, Abouzeid AM, El-Maadawy K, Khalid AM, El-Sherif RE (2016) Mineral industry in Egypt part II non-metallic commodities: silica ores. *J Min World Express (MWE)* 5. <https://doi.org/10.14355/mwe.2016.05.002>
  21. Shaban M, Abukhadra MR (2016) Enhancing the technical qualifications of Egyptian white sand using acid leaching; response surface analysis and optimization. *Int J Miner Process Extr Metall* 1(4):33–40. <https://doi.org/10.11648/j.ijmpem.20160104.13>
  22. Tuncuk A, Akcil A (2016) Iron removal in production of purified quartz by hydrometallurgical process. *Int J Miner Process* 153:44–50. <https://doi.org/10.1016/j.minpro.2016.05.021>
  23. EL Sayed MA, Fathy WM, Salleh AM, Moharam MR, Ibrahim SS (2018) Processing of Wadi Qena kaolinitic white sands by selective dispersion and leaching for industrial uses. *J Al-Azhar Univ Eng Sect* 13(47):530–545. <https://doi.org/10.21608/aej.2018.19059>
  24. Hafez NAAE, Ibrahim GE-DA, Khatita AMA, El-hariri TYMA, Mousa AS, Mohamed NI, Arafat AM (2016) Practical application to increase the additional value for the white sand as environmental safe product of the wadi El-Dakhl, Eastern Desert, Egypt. *Int J Innov Sci Technol* 3(5). [https://ijiset.com/vol3/v3s5/IJISSET\\_V3\\_I5\\_61.pdf](https://ijiset.com/vol3/v3s5/IJISSET_V3_I5_61.pdf)
  25. Muhammad AF, Salmawy MSE, Abdelaal AM (2013) Potential for upgrading El-Nakheil oil shale by froth flotation. *Oil Shale* 30(1):48–59. <https://doi.org/10.3176/oil.2013.1.05>
  26. Muhammad AF, Salmawy MSE, Abdelaal AM, Sameah S (2011) EL-Nakheil oil shale: material characterization and effect of acid leaching. *Oil Shale* 28(4):528–547. <https://doi.org/10.3176/oil.2011.4.06>
  27. Peng X, Yang G, Shi Y, Zhou Y, Zhang M, Li S (2020) Box-Behnken design based statistical modeling for the extraction and physicochemical properties of pectin from sunflower heads and the comparison with commercial low-methoxyl pectin. *Sci Rep* 10(1):3595. <https://doi.org/10.1038/s41598-020-60339-1>
  28. Salem M, Shoaib AM, Ibrahim AFM (2021) Simulation of a natural gas steam reforming plant for hydrogen production optimization. *Chem Eng Technol* 44(9):1651–1659. <https://doi.org/10.1002/ceat.202100123>
  29. Ibrahim GE-DA, Mousa AS, El-hariri TYMA, Hassnien IM, zakzouk NI (2016) New industrial use of Egyptian white sands from Wadi El- Dakhl area, Eastern Desert, Egypt. *Int J Innov Sci Technol* 3(1). [https://ijiset.com/vol3/v3s1/IJISSET\\_V3\\_I1\\_71.pdf](https://ijiset.com/vol3/v3s1/IJISSET_V3_I1_71.pdf)
  30. Madhavaraju J, Barragán JCGy, Hussain SM, Mohan SP (2009) Microtextures on quartz grains in the beach sediments of Puerto Peñasco and Bahía Kino, Gulf of California, Sonora, Mexico. *Rev Mex Cienc Geol* 26:367–379
  31. Ben Salah I, M'Barek Jemai MB, Sdiri A, Boughdiri M, Karoui N (2016) Chemical and technological characterization and beneficiation of Jezza sand (North West of Tunisia): potentialities of use in industrial fields. *Int J Miner Process* 148:128–136. <https://doi.org/10.1016/j.minpro.2016.01.016>
  32. Hao C, Chu M, Wang L, Zhou L (2020) The effect of preparation conditions on microbubble flotation process of ultra clean coal using box Behnken design model. *ChemistrySelect* 5(5):1767–1775. <https://doi.org/10.1002/slct.201902447>

33. Lee SO, Tran T, Jung BH, Kim SJ, Kim MJ (2007) Dissolution of iron oxide using oxalic acid. *Hydrometallurgy* 87(3):91–99. <https://doi.org/10.1016/j.hydromet.2007.02.005>
34. Lee SO, Tran T, Park YY, Kim SJ, Kim MJ (2006) Study on the kinetics of iron oxide leaching by oxalic acid. *Int J Miner Process* 80(2):144–152. <https://doi.org/10.1016/j.minpro.2006.03.012>
35. Hernández Hernández RA, Legorreta García F, Hernández Cruz LE, Bedolla Jacuinde A (2015) Kaolin bleaching by leaching using phosphoric acid solutions. *J J Mex Chem Soc* 59:198–201
36. Al-Sogair F, Marafie HM, Shuaib NM, Youngo HB, El-Ezaby MS (2002) Interaction of phosphate with Iron(III) in acidic medium, equilibrium and kinetic studies. *J Coord Chem* 55(9):1097–1109. <https://doi.org/10.1080/0095897021000010053>
37. Banza AN, Quindt J, Gock E (2006) Improvement of the quartz sand processing at Hohenbocka. *Int J Miner Process* 79(1):76–82. <https://doi.org/10.1016/j.minpro.2005.11.010>
38. Li F, Jiang X, Zuo Q, Li J, Ban B, Chen J (2020) Purification mechanism of quartz sand by combination of microwave heating and ultrasound assisted acid leaching treatment. *Silicon* 13:531–541. <https://doi.org/10.1080/08827508.2013.825614>
39. EL-Wekeil SS, Gaafar FSh (2014) Characterization and economic potential of the white sandstones of the Naqus Formation in Wadi Qena, Northern Eastern Desert, Egypt. *Middle East J Appl Sci* 4(2):392–408

**Publisher's Note** Springer Nature remains neutral with regard to jurisdictional claims in published maps and institutional affiliations.